

Toward a Low-Cost Perception System in Autonomous Vehicles: A Spectrum Learning Approach

Mohammed Alsakabi¹, Aidan Erickson¹, John M. Dolan², Ozan K. Tonguz¹
¹Department of Electrical and Computer Engineering, College of Engineering
²The Robotics Institute, School of Computer Science
Carnegie Mellon University, Pittsburgh, PA, United States
{malsakabi, aerickson}@cmu.edu, {jdolan, tonguz}@andrew.cmu.edu

Abstract—We present a cost-effective new approach for generating denser depth maps for Autonomous Driving (AD) and Autonomous Vehicles (AVs) by integrating the images obtained from deep neural network (DNN) 4D radar detectors with conventional camera RGB images. Our approach introduces a novel pixel positional encoding algorithm inspired by Bartlett’s spatial spectrum estimation technique. This algorithm transforms both radar depth maps and RGB images into a unified pixel image subspace called the Spatial Spectrum, facilitating effective learning based on their similarities and differences. Our method effectively leverages high-resolution camera images to train radar depth map generative models, addressing the limitations of conventional radar detectors in complex vehicular environments, thus sharpening the radar output. We develop spectrum estimation algorithms tailored for radar depth maps and RGB images, a comprehensive training framework for data-driven generative models, and a camera-radar deployment scheme for AV operation. Our results demonstrate that our approach also outperforms the state-of-the-art (SOTA) by 27.95% in terms of Unidirectional Chamfer Distance (UCD).

I. INTRODUCTION

Autonomous Vehicles (AV) employ various sensors for comprehensive navigation and environmental perception, each contributing distinct advantages and limitations. RGB cameras are attractive due to their affordability and high accuracy in optimal lighting conditions but they struggle in low-visibility scenarios like darkness, heavy rain, or fog, which impede obstacle detection. Lidars offer precise 3D mapping and depth measurements, yet they consume high power, are susceptible to adverse weather conditions, and sometimes require mechanical parts for rotational scanning, raising the overall manufacturing and operational costs. Radars, however, stand out for their robustness in adverse weather, cost-effectiveness, low power consumption, and can offer a theoretical angular resolution comparable to lidars.

Automotive radars measure range, azimuth, and velocity, with 4D radars adding elevation to their traditional measurements. Unlike 3D radars, 4D radars are capable of estimating object heights without using speculative models. For such radars, extracting precise angular information involves a two-stage process: spatial spectrum estimations followed by Constant False Alarm Rate (CFAR) detectors like cell-

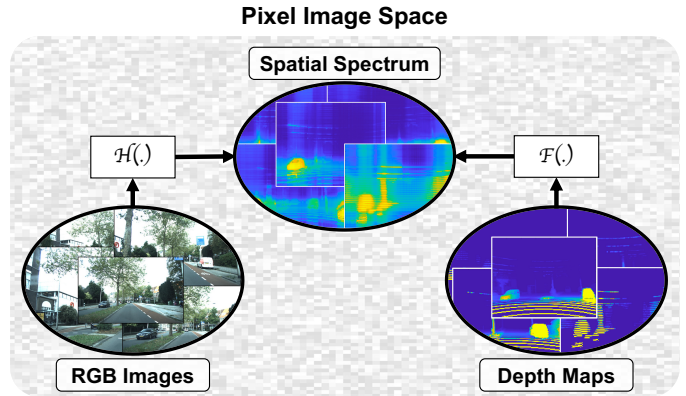


Fig. 1: Conceptual figure depicting the proposed spectrum-based transformation. The ‘RGB’ and ‘Depth Maps’ subspaces represent natural images captured by conventional cameras and the windshield view depth maps that lidars and radars produce, respectively. The ‘Spatial Spectrum’ subspace includes the special frequency 2D spectrum of bases that constitute images in the other subspaces.

averaging CFAR (CA-CFAR) and order-statistic CFAR (OS-CFAR) [1]. However, these conventional methods struggle in complex vehicular settings, producing sparse point clouds that limit accurate environmental representation [2]. To address these limitations, data-driven approaches using deep neural networks (DNNs) have been reported [3]–[5]. For instance, [5] employs a ResNet18 network [6] trained on dense lidar point clouds, generating denser radar point clouds that more accurately represent object shapes and sizes.

In this paper, we introduce a data-driven approach for generating radar depth maps by integrating radar point clouds with camera images. Leveraging the similar field-of-view (FoV) between radar and camera images, employing a non-linear frequency pixel positional encoding algorithm and Bartlett’s spatial spectrum estimation [7] transforms radar depth maps and camera RGB images into a shared spatial spectrum subspace, as shown in Figure 1. This transformation can resolve the differences between the 4D radar image and camera images, thus enabling spectrum-based learning. The method enables the use of high-resolution cameras to effectively train radar depth map generators. After this off-line training, the

4D radar model can operate independently of the camera, generating sharper and denser depth maps that are critical for perception, tracking, and rendering in AVs. Our contributions can be summarized as:

- We propose a pixel positional encoding algorithm that helps resolve the differences between a 4D radar image and RGB camera image, thus enabling spectrum-based learning for 4D radar images.
- We present experimental results for high-resolution spectrum estimations and depth map generations. Our results show that our approach is capable of producing qualitatively sharp depth maps and significantly outperforms the state-of-the-art (SOTA), resulting in a reduction of 21.13%, 7.9% and 27.95% in Mean Absolute Error (MAE), Relative Absolute Error (REL), and Unidirectional Chamfer Distance (UCD), respectively, which is quite significant. [8]. We also show that the estimated spectrum of camera and radar images results in an increase of the Pearson correlation and mutual information by a factor of 3.88 and 76.69, respectively.

II. RELATED WORK

A. Datasets

This work requires 4D radar data that include raw measurements in order to apply novel DNN detectors. Here, we review available 4D radar datasets.

The RaDelft, VoD, and K-Radar datasets are critical resources for automotive radar research, each offering unique capabilities. The RaDelft dataset provides synchronized 4D radar, lidar, camera, and odometry data from Delft, Netherlands, and has been used in deep learning to replicate lidar-like expressiveness with radar input [5]. Similarly, the VoD dataset integrates camera, BEV S3 lidar, 4D radar, and odometry data, offering annotations and bounding boxes for object detection, making it ideal for multimodal research and downstream tasks [9]. The K-Radar dataset serves as a benchmark for object detection and classification with pre-processed radar data like range Doppler and range-angle maps, along with ground truth annotations. However, it lacks raw 4D radar signals, limiting its application in workflows requiring unprocessed radar data [10]. In this work, we are using the RaDelft DL detector dataset, as VoD and K-radar do not provide raw radar signals that are sufficient for applying the detector developed in [5].

B. Multimodal Data Fusion for Depth Map Generation

Several advanced methods leverage radar and camera fusion to enhance autonomous driving perception tasks. For example, [11] introduces a two-stage pixel-level fusion method for depth completion, where radar-to-pixel association in the first stage maps radar returns to pixels using lidar-generated ground truth, and the second stage fuses this output with camera images featuring projected 3D radar point clouds. Similarly, [12] adopts a two-stage approach that uses RadarNet to generate a confidence map from RGB images and noisy 3D radar point clouds in the first stage, followed by depth map enhancement using the confidence map and RGB images. In contrast, [13]

proposes a four-stage framework for dense depth estimation that enhances monocular depth prediction with accurate metric scale information derived from sparse 3D radar data, using global scale alignment, transformer-based quasi-dense scale estimation, and local refinement. Expanding on these concepts, [14] develops a semantic-guided depth completion framework that incorporates a Radar Point Correction Module (RPCM) for radar refinement, a Semantic Divide-and-Conquer Module (SDCM) for category-specific tasks, and a Region Depth Diffusion Module (RDDM) for further depth refinement. Additionally, [15] targets 3D occupancy prediction by directly processing radar tensors with Doppler bin descriptors and spherical-based feature encoding, excelling in adverse weather conditions on the K-Radar dataset.

Unlike the aforementioned methods, our approach shows that using the DNN detector model in [5] as a module, we can improve the depth maps generated by further training this model with images generated by cheap cameras. This paves the way for eliminating the use of lidars for real time perception in AVs.

III. BACKGROUND

A. Radar Detectors

Radar detectors process signals to differentiate targets from noise by applying a decision threshold, comparing the signal strength to a predefined value, and outputting results as point clouds. Conventional radar detectors, like CA-CFAR and OS-CFAR, aim to maintain a consistent false alarm rate by dynamically adjusting decision thresholds based on surrounding noise and clutter. CA-CFAR works well in homogeneous environments but struggles with the heterogeneity of vehicular surroundings. OS-CFAR handles heterogeneous environments but requires precise prior knowledge of target numbers, which might be challenging to estimate. However, a recent deep learning-based radar detector by [5] trained on lidar point clouds addresses these limitations, but struggles with sparse representations of its surroundings, compared to lidar. In this work, we produce denser depth maps using these sparse representations.

B. Bartlett's Algorithm for Spatial Power Spectrum Estimation

Bartlett's algorithm, also known as periodogram averaging [7], is used in signal processing and time series analysis to estimate the power spectral density of a random sequence. It divides the sequence into M overlapping segments, computes their periodograms, and averages them, with the number of segments being proportional to the spectral resolution. For received signals at spatially distant receptors, like signals received at different camera physical pixels or signals received in multi-antenna wireless systems, the M segments correspond to the signals received at the M receptor. The time difference between segments introduces a phase shift proportional to the spatial frequency ω , referenced against the complex sinusoidal signal at the first receptor [16], described as:

$$x_1(n) = e^{-j\omega n}, n = 0, 1, \dots, N \quad (1)$$

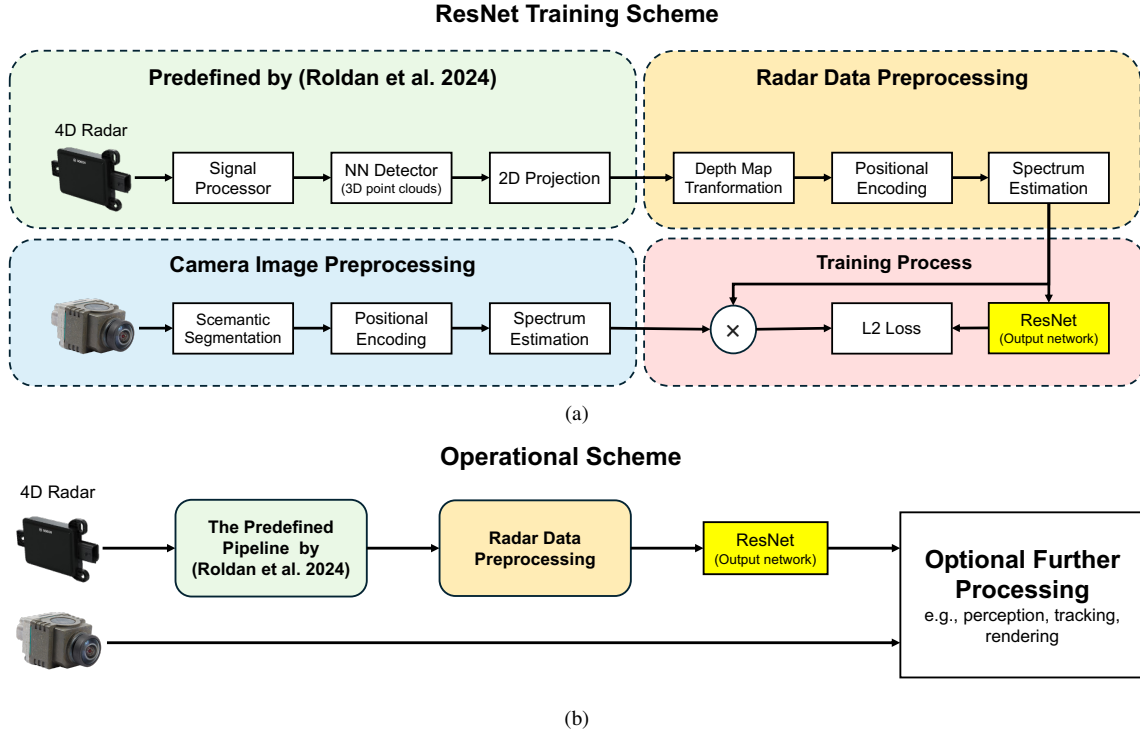


Fig. 2: The pipeline for our proposed method: (a) The offline network training scheme is divided into four modules: the predefined radar signal processing and detection (point-clouds extractor) by [5], the pre-processing of camera and radar data defined under 'Proposed Approach', and the training process which takes the 'Radar Data Pre-processing' output as input and the filtered 'Camera Image Pre-processing' output as the ground truth for training. (b) The proposed operational deployment of the trained network in (a) considering the required lower-level processes, where radar and camera work independently of each other and provide data for any required further process.

where N is the number of samples in the signal. Assuming that we have M segments, each segment has a time delay that is translated into a phase shift in $x_1(n)$, expressed as:

$$x_m(n) = x_1(n)e^{-jm\phi} = e^{-j(\omega n + m\phi)}, m = 0, 1, \dots, M - 1 \quad (2)$$

Hence, the M segments matrix $\mathbf{S} \in \mathbb{C}^{N \times M}$ is found as:

$$\mathbf{S} = [\mathbf{x}_1 \quad \mathbf{x}_2 \quad \dots \quad \mathbf{x}_M] \quad (3)$$

Since we are computing the spatial power spectrum, our goal is to calculate the spectrum of the signal that is described by relative phases between segments, which can be found in the covariance matrix $\mathbf{C} \in \mathbb{C}^{M \times M}$ of \mathbf{S} as:

$$\mathbf{C} = \frac{1}{N} \mathbf{S}^H \mathbf{S} \quad (4)$$

where H denotes the Hermitian or complex conjugate. Therefore, the power spectral density at ϕ , $P(\phi)$, is found as:

$$P(\phi) = \mathbf{a}(\phi)^H \mathbf{C} \mathbf{a}(\phi) \quad (5)$$

where $\mathbf{a}(\phi) = [1 \quad e^{-j\phi} \quad e^{-j2\phi} \quad \dots \quad e^{-j(M-1)\phi}]^T$ is our basis vector. Note that the choice of basis vector depends on the application, pattern of interest, and desired resolution [17]. A different basis vector is used for our proposed approach, defined in the next section.

IV. PROPOSED APPROACH

Unlike lidars, 4D imaging radars used in AV suffer from sparse scene representations. Our goal in this work is to bypass lidars and produce sharp 4D radar depth maps by passing the radar output to a data-driven depth map generator. Since the camera RGB images have different characteristics from radar depth maps (i.e., they come from different pixel image subspaces), we propose to compute their unified, constitutive basis vectors and transform them into their spatial spectrum representations using Bartlett's algorithm. This bridges the gap between their original characteristics. With non-linear frequency progression basis vectors, we propose to encode the semantic segmentations of camera images and their corresponding radar depth maps to estimate their spatial spectrum. Interestingly, the spatial spectrum of both images includes frequency components proportional to M caused by spectral leakage. These frequency components complete the depth for sparse point clouds, as well as introduce frequency bias that helps with fitting highly oscillatory data (the sharp camera images), as shown in Figure 3 [18]. Figure 2a depicts this transformation and network training pipeline, while 2b shows the deployment pipeline for real-time operation, noting that the 4D radar and camera work independently but synchronously.

A. Pixel Positional Encoding and Spectrum Estimation

This encoding method aims to facilitate the transformation into the spatial spectrum of both the radar and camera images.

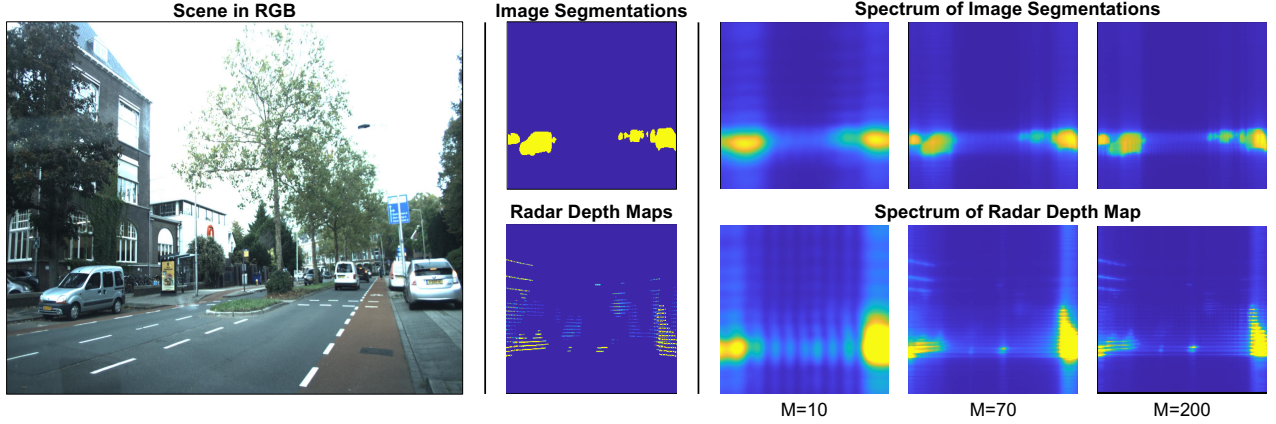


Fig. 3: Results for $M = 10, 70$ and 200 , and $\Phi = \Theta = (-70, 70)$ against the original RGB scene on the left.

Fast implementation of this encoding process starts with an initialization of a non-linear phase progression, complex sinusoidal basis vectors for M segments for horizontal and vertical axes, ϕ and θ . Our basis functions differ from the standard Fourier basis functions, since we require higher resolution for the output [17]. For that, we change the phase progression across basis functions from standard linear to non-linear, resulting in changing frequency across receptors. This changing frequency leads to higher resolution spectrum [1]. Our segments are described as:

$$x(m, \phi_n) = e^{-j\pi m \sin(\phi_n)}, x(m, \theta_k) = e^{-j\pi m \sin(\theta_k)} \quad (6)$$

where m is the segment index, noting that M is proportional to spectrum resolution, and ϕ_n and $\theta_k \in \Phi$ and Θ are variation angles from the set $(-90, 90)$ with lengths N and K , respectively. The covariance matrices of every ϕ and θ are defined as $\mathbf{C}(\Phi)$ and $\mathbf{C}(\Theta) \in \mathbb{C}^{N \times N}$ and $\mathbb{C}^{K \times K}$, in which each of their rows represents the periodograms $\mathbf{y}(\phi_n)$ and $\mathbf{y}(\theta_k)$. The joint 2D periodogram is:

$$\mathbf{Y}(\phi_n, \theta_k) = \mathbf{y}(\theta_n)^T \mathbf{y}(\phi_k) \quad (7)$$

To calculate the final 2D spatial power spectrum $\mathbf{P} \in \mathbb{R}^{N \times K}$ for an input image \mathbf{I} , we iteratively encode all pixels of \mathbf{I} and calculate $P(n, k)$ as:

$$P(n, k) = \sum_{n=0}^{N-1} \sum_{k=0}^{K-1} |\mathbf{Y}(\phi_n, \theta_k) \circ \mathbf{I}| \quad (8)$$

where \circ denotes an element-wise multiplication. Experimental results are presented in the next section.

B. Radar Data Preprocessing

This module conditions the DNN detector's depth map, \mathbf{I}_{radar} , in the predecessor radar pipeline. The objective is to transform 2D depth maps into a spatial spectrum representation of its constitutional bases, \mathbf{P}_{radar} , to satisfy the input characteristics in the following module, the 'Training Process'. This process of spatial spectrum estimation is defined as $\mathcal{F}(\mathbf{I}, M)$, noting that M is proportional to the output resolution.

$$\mathbf{P}_{radar} = \mathcal{F}(\mathbf{I}_{radar}, M_{radar}) \quad (9)$$

C. Camera Image Preprocessing

In order to obtain the spatial spectrum representations for objects of interest, we transform the RGB image, \mathbf{I}_{cam} , into its semantic segmentations, \mathbf{Seg} , considering that this is highly dependent on the semantic segmentation accuracy and classes of the model in use. We use Deeplab v3 [19] with ResNet101 [6] trained on the PASCAL Visual Object Classes (VOC) 2012 dataset [20]. We then transform the semantic image into its spatial spectrum representation \mathbf{P}_{cam} through $\mathcal{H}(\mathbf{I}, M)$, which is the process of spatial spectrum estimation of camera images.

$$\mathbf{P}_{cam} = \mathcal{H}(\mathbf{I}_{cam}, M_{cam}) = \mathcal{F}(\mathbf{Seg}, M_{cam}) \quad (10)$$

Note that we require $M_{cam} > M_{radar}$ so that the radar spectrum images have a lower resolution, which leaves room for enhancement with deep learning models.

D. Network Training Process

This module focuses on training a generative model that produces a denser and contour-accurate version of \mathbf{P}_{radar} . As there are some objects captured by the semantic segmentation model that are not detectable by radar, and vice versa, element-wise multiplication produces the mutuality between both spectrum images which, thereafter, is fed into the learning as ground truth for training a ResNet, being optimized to reduce the difference through L2 loss. The process is described as:

$$\mathbf{P}_{radar} \circ \mathbf{P}_{cam} = \text{ResNet}(\mathbf{P}_{radar}) \quad (11)$$

V. EXPERIMENTAL RESULTS AND ANALYSIS

We apply the proposed approach to the Radelft dataset's RGB images and radar depth maps of Scene 2, which includes 3400 frames. We performed two main experiments: a test of the spatial spectrum generation using the proposed approach and an enhancement of these spatial spectrum images.

We evaluate the performance of the data preprocessing by computing the Pearson correlation and mutual information metrics between the generated spectrums of RGB pixel semantic segmentation and the corresponding radar depth maps

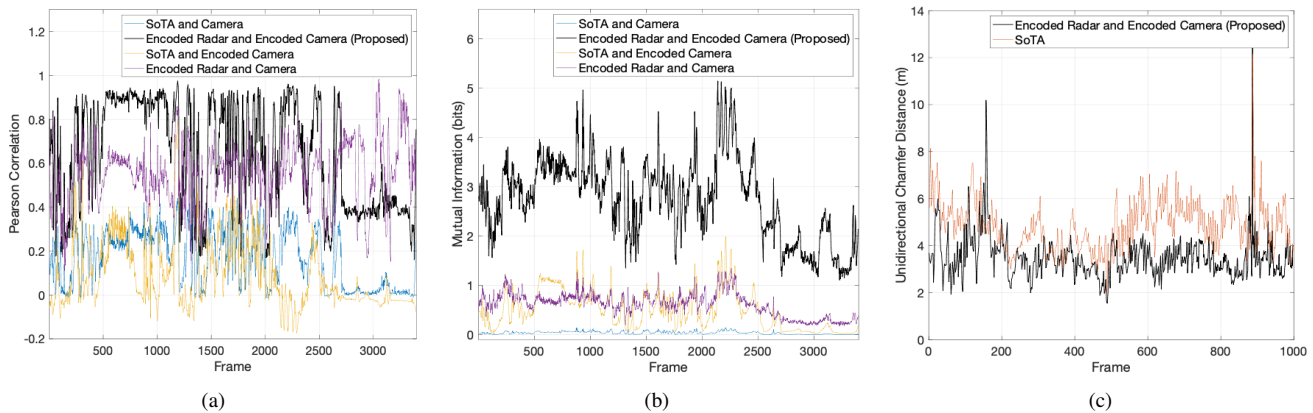


Fig. 4: (a) Correlation and (b) mutual information between several depth map pairs. ‘SoTA’ refers to depth map obtained by [5] while ‘Encoded’ refers to the spectrum of encoded images using the described bases.

for $M_{radar} = 50$ and $M_{cam} = 200$, noting that a higher correlation value indicates a smaller discrepancy between the images, while mutual information indicates the learning potential of one modality from the other.

The performance of the depth map generation is measured by MAE, REL, RMSE, and UCD against the lidar point clouds and depth maps. MAE evaluates the average magnitude of errors in predictions, providing a straightforward measure of accuracy. REL normalizes the error by comparing it to the mean of the actual values, offering insight into the relative performance of the predictions. RMSE emphasizes larger errors by squaring the differences before averaging, making it sensitive to outliers. UCD measures the geometric similarity between the generated depth maps and the ground truth point clouds by calculating the average distance from each predicted point to its closest corresponding point in the lidar data. As our generation is dependent on semantic segmentations, this approach eliminates the average distance inflation that is caused by detectable object discrepancies between the semantic segmentation model, and radar and lidar point clouds when using Bidirectional Chamfer Distance (BCD).

A. Data Preprocessing

Our data preprocessing pipeline includes an input data conditioning sub-module followed by the proposed encoding approach explained in the previous sections. We performed experiments for $M = 10, 50, 70, 200$ and $\Phi = \Theta = (-70, 70)$ degrees that truncate significant spectrum leakage at higher angles. The radar input is a simple data structure transformation from projected 3D point clouds coordinates to 2D depth maps with the pixel value being inversely proportional to depth. We test our data preprocessing against Pearson correlation and mutual information. The higher value of Pearson correlation represents a stronger linear relationship between the two variables, while the higher value of mutual information indicates a greater reduction in the entropy when predicting one variable from another.

In Figure 3, one can observe that a greater M produces higher-resolution images that preserve the contours of objects. The ripples in both horizontal and vertical axes are due

to spectral leakage. Figure 4a plots the Pearson correlation values per frame between the camera and radar modalities for $M_{radar} = 50$ and $M_{cam} = 200$. It also shows that the correlation is still higher when both radar depth map and camera semantic segmentation are encoded with the proposed approach. It also shows that the correlation is significantly higher for single modality encoding. Figure 4b shows that mutual information is significantly improved when we encode both modalities. It also shows that mutual information is still significantly improved when we encode only a single modality.

Tables I and ?? show the averages (mean values) of the plots in Figures 4a and 4b. The results show that there are improvements by factors of 3.88 and 76.69 in Pearson correlation and mutual information, respectively.

	I_{cam}	P_{cam}
I_{radar}	0.1646	0.5503
P_{radar}	0.0809	0.6396

TABLE I: Average Pearson Correlation for different pairs.

	I_{cam}	P_{cam}
I_{radar}	0.0359	0.6117
P_{radar}	0.4863	2.7533

TABLE II: Average Mutual Information for different pairs.

B. Depth Map Generation

The depth map generation is achieved with the ResNet101 network trained as described in the previous section with $M_{cam} = 200$, $M_{radar} = 20$ and $\Phi = \Theta = (-70, 70)$. The ResNet101 is trained for 10,000 epochs while the input data are compressed with the natural logarithm to make different features comparable in terms of scale. Qualitatively, from the results in Figure 5, one can observe that the intensity locations in the radar depth maps are comparable to locations in camera spectrum images. Also, the output depth maps from the ResNet101 show object contours clearly compared to the original radar depth map. However, the magnitude of the ripples is significantly higher due to the logarithmic feature compression used at the input, which can be rescaled by exponentiation.

Quantitatively, we measure the performance of the output with MAE, REL, RMSE, and UCD. Specifically for UCD, we transform the spectrum images into 3D point clouds (in which the depth is inversely proportional to the pixel value) and apply the calculations. Table III presents the results for

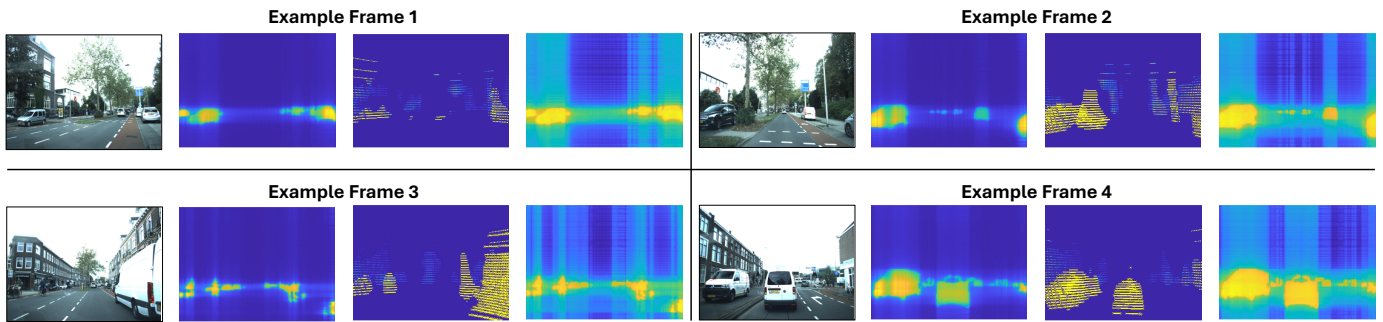


Fig. 5: Results from the training module for four example frames. From left to right for each example frame: Scene in RGB, Camera spatial spectrum (\mathbf{P}_{cam}), original radar depth map, output from trained ResNet101. In each of the 4 frames, observe that our approach leads to sharper depth maps.

different methods including the state-of-the-art (SOTA) DNN detector [5] and the OS-CFAR. Figure 4c shows the per frame UCD for our method and SOTA. We observe that our approach improves MAE, REL, UCD by 21.13%, 7.9% and 27.95%, respectively. However, the performance degrades by 12% in terms of RMSE. We believe that this is due to the fact that, compared to other approaches, our generated depth maps are dense, inflating the RMSE result as there are gaps in the corresponding lidar depth maps.

Method	MAE	REL	RMSE	UCD (m)
Proposed Approach	0.026	0.025	0.111	3.48
SOTA DNN	0.033	0.027	0.099	4.83
OS-CFAR	0.029	0.152	0.258	18.02
Improvement (%)	21.13	7.9	-12	27.95

TABLE III: MAE, REL, RMSE, and UCD for different methods

VI. CONCLUSION

This paper introduces a novel method for generating 4D radar depth maps for autonomous vehicles by integrating depth maps from DNN-based radar detectors with camera images using a positional encoding inspired by Bartlett’s algorithm. This approach converts radar point clouds and camera images into a shared spectrum representation, enhancing their correspondence and enabling the training of radar image generators with high-resolution camera data. The method achieves a significant improvement of 27.95% in unidirectional Chamfer distance compared to the state-of-the-art, delivering more accurate and denser radar-generated depth maps than traditional CFAR detectors. By offering a highly trained 4D Radar, the presented approach holds the promise of making perception in AVs much more cost-effective when used in conjunction with cheap cameras in real time, by avoiding the expense of Lidar.

REFERENCES

- [1] M. A. Richards, J. Scheer, W. A. Holm, and W. L. Melvin, “Principles of modern radar,” in *Principles of Modern Radar*. Citeseer, 2010, ch. 16.
- [2] M. A. U. Khan, D. Nazir, A. Pagani, H. Mokayed, M. Liwicki, D. Stricker, and M. Z. Afzal, “A comprehensive survey of depth completion approaches,” *Sensors*, vol. 22, no. 18, p. 6969, 2022.
- [3] D. Brodeski, I. Bilik, and R. Giryes, “Deep radar detector,” in *2019 IEEE Radar Conference (RadarConf)*. IEEE, 2019, pp. 1–6.
- [4] Y. Cheng, J. Su, M. Jiang, and Y. Liu, “A novel radar point cloud generation method for robot environment perception,” *IEEE Transactions on Robotics*, vol. 38, no. 6, pp. 3754–3773, 2022.
- [5] I. Roldan, A. Palffy, J. F. Kooij, D. M. Gavrilu, F. Fioranelli, and A. Yarovoy, “See further than cfar: a data-driven radar detector trained by lidar,” *arXiv preprint arXiv:2402.12970*, 2024.
- [6] L.-C. Chen, G. Papandreou, F. Schroff, and H. Adam, “Rethinking atrous convolution for semantic image segmentation,” *arXiv preprint arXiv:1706.05587*, 2017.
- [7] M. S. Bartlett, “Smoothing periodograms from time-series with continuous spectra,” *Nature*, vol. 161, no. 4096, pp. 686–687, 1948.
- [8] J. Zhang, X. Chen, Z. Cai, L. Pan, H. Zhao, S. Yi, C. K. Yeo, B. Dai, and C. C. Loy, “Unsupervised 3d shape completion through gan inversion,” in *Proceedings of the IEEE/CVF Conference on Computer Vision and Pattern Recognition*, 2021, pp. 1768–1777.
- [9] A. Palffy, E. Pool, S. Baratam, J. F. P. Kooij, and D. M. Gavrilu, “Multi-class road user detection with 3+1d radar in the view-of-delft dataset,” *IEEE Robotics and Automation Letters*, vol. 7, no. 2, pp. 4961–4968, 2022.
- [10] D.-H. Paek, S.-H. Kong, and K. T. Wijaya, “K-radar: 4d radar object detection for autonomous driving in various weather conditions,” *Advances in Neural Information Processing Systems*, vol. 35, pp. 3819–3829, 2022.
- [11] Y. Long, D. Morris, X. Liu, M. Castro, P. Chakravarty, and P. Narayanan, “Radar-camera pixel depth association for depth completion,” in *Proceedings of the IEEE/CVF Conference on Computer Vision and Pattern Recognition*, 2021, pp. 12 507–12 516.
- [12] A. D. Singh, Y. Ba, A. Sarker, H. Zhang, A. Kadambi, S. Soatto, M. Srivastava, and A. Wong, “Depth estimation from camera image and mmwave radar point cloud,” in *Proceedings of the IEEE/CVF Conference on Computer Vision and Pattern Recognition*, 2023, pp. 9275–9285.
- [13] H. Li, Y. Ma, Y. Gu, K. Hu, Y. Liu, and X. Zuo, “Radarcam-depth: Radar-camera fusion for depth estimation with learned metric scale,” *arXiv preprint arXiv:2401.04325*, 2024.
- [14] Z. Li, Y. Song, F. Ai, C. Song, and Z. Xu, “Semantic-guided depth completion from monocular images and 4d radar data,” *IEEE Transactions on Intelligent Vehicles*, 2024.
- [15] F. Ding, X. Wen, Y. Zhu, Y. Li, and C. X. Lu, “Radarocc: Robust 3d occupancy prediction with 4d imaging radar,” *arXiv preprint arXiv:2405.14014*, 2024.
- [16] A. Dixit and et al., “Detection and localization of targets using millimeter wave radars: An experimental study,” in *2021 IEEE International Conference on Electronics, Computing and Communication Technologies (CONECT)*, 2021, pp. 1–6.
- [17] M. B. Priestley, *Spectral analysis and time series*. Academic press London, 1981, vol. 890.
- [18] Z.-Q. J. Xu, Y. Zhang, and T. Luo, “Overview frequency principle/spectral bias in deep learning,” *Communications on Applied Mathematics and Computation*, pp. 1–38, 2024.
- [19] S. C. Yurtkulu, Y. H. Şahin, and G. Unal, “Semantic segmentation with extended deeplabv3 architecture,” in *2019 27th Signal Processing and Communications Applications Conference (SIU)*. IEEE, 2019, pp. 1–4.
- [20] M. Everingham and et al., “The pascal visual object classes (voc) challenge,” *International Journal of Computer Vision*, vol. 88, no. 2, pp. 303–338, Jun. 2010.